Photosynthetic reaction center as a quantum heat engine

Konstantin E. Dorfman[a,b,c,1], Dmitri V. Voronine[a,b,1], Shaul Mukamel[c], and Marlan O. Scully[a,b,d]

[a]Texas A&M University, College Station, TX 77843-4242; [b]Princeton University, Princeton, NJ 08544; [c]University of California, Irvine, CA 92697-2025; and [d]Baylor University, Waco, TX 76798

Edited by Graham R. Fleming, University of California, Berkeley, CA, and approved November 15, 2012 (received for review July 26, 2012)

Two seemingly unrelated effects attributed to quantum coherence have been reported recently in natural and artificial light-harvesting systems. First, an enhanced solar cell efficiency was predicted and second, population oscillations were measured in photosynthetic antennae excited by sequences of coherent ultrashort laser pulses. Because both systems operate as quantum heat engines (QHEs) that convert the solar photon energy to useful work (electric currents or chemical energy, respectively), the question arises whether coherence could also enhance the photosynthetic yield. Here, we show that both effects arise from the same population–coherence coupling term which is induced by noise, does not require coherent light, and will therefore work for incoherent excitation under natural conditions of solar excitation. Charge separation in light-harvesting complexes occurs in a pair of tightly coupled chlorophylls (the special pair) at the heart of photosynthetic reaction centers of both plants and bacteria. We show the analogy between the energy level schemes of the special pair and of the laser/photocell QHEs, and that both population oscillations and enhanced yield have a common origin and are expected to coexist for typical parameters. We predict an enhanced yield of 27% in a QHE motivated by the reaction center. This suggests nature-mimicking architectures for artificial solar energy devices.

photosynthesis | quantum biology | population oscillations | quantum coherence

According to the laws of quantum thermodynamics, quantum heat engines (QHEs) convert hot thermal radiation into low-entropy useful work (1, 2). The ultimate efficiency of such QHEs is usually governed by a detailed balance between absorption and emission of the hot pump radiation (3). The laser is an example of a QHE, which can use incoherent pump (heat) radiation to produce highly coherent (low-entropy) light (Fig. 1 *A* and *B*). Moreover, it was demonstrated both theoretically and experimentally that noise-induced quantum coherence (4) can break detailed balance and yield lasers without population inversion (5) and/or with enhanced efficiency (Fig. 1*C*).

Recently it has been shown that quantum coherence can, in principle, enhance the efficiency of a solar cell or a photodetector (6–10). This photocell QHE (Fig. 1*D*) can be described by the same model as the laser QHE (Fig. 1*E*) and obeys similar detailed balance physics. To use the broad solar spectrum and eliminate phonon loss, we separate solar flux into narrow frequency intervals and direct it onto a cell array where each of the cells has been prepared to have its band gap equal to that photon energy (7). In particular, Shockley and Queisser (11) invoked detailed balance to show that the open-circuit voltage of a photocell is related to the energy input of a "hot" monochromatic thermal light by the Carnot factor. However, just as in the case of the laser, we can, in principle, break detailed balance by inducing coherence (Fig. 1*F*), which can enhance the photocell efficiency (9, 10).

Other recent papers investigated the common ground between photovoltaics and photosynthetic light harvesting (12, 13). Various models addressed the high efficiency of energy transfer in photosynthetic antennae (14–19) and the mechanisms of charge separation in reaction centers (12, 20–22). Furthermore, quantum coherence effects, e.g., photon echo, have been observed in a series of interesting photosynthesis experiments (23–30). Oscillations of exciton population signals in the 2D photon echo (rephasing) spectra have been predicted (31) and directly observed (32) as evidence of quantum transport. However, because multidimensional spectroscopy uses coherent laser radiation as a source of quantum coherence, the quantum effects that might be observed under natural conditions of excitation by incoherent solar light are still an open issue.

Coherent versus incoherent energy transfer has long been studied in molecular crystals and aggregates (33–35). It is well established that the interplay between exciton coupling and energetic disorder controls the extent of exciton delocalization, which in turn determines the nature of transport (36). Coherent effects become more prominent as the excitons become more delocalized. Recent femtosecond experiments in photosynthetic complexes have revived the interest in the same issues. Oscillatory temporal features in 2D spectra have been initially attributed to electronic coherence but growing evidence indicates that this could be due as well to strongly coupled vibronic motions (37–40). The simplest approach to energy transfer is based on the Redfield equations that treat the system/bath coupling perturbatively to second order. They are invariant to the exciton basis and can be applied to localized and delocalized excitons alike (41). The Förster theory of energy transfer and the Marcus theory of charge transfer assume localized states. Like the Redfield equations they treat off-diagonal couplings perturbatively but include diagonal bath fluctuations (polaron effects) to high order. Both theories can be derived in a very transparent way by using a unified formalism of bath fluctuations based on the cumulant expansion (20, 42).

We apply the physics of the laser and photocell described above to investigate these effects in a QHE inspired by photosynthetic complexes. In the model of Fig. 2*B*, the broad solar spectrum can be used by various photosynthetic antennae complexes which transfer energy to the reaction center. The antennae absorb broadband light in the visible range and relax to the bottom of the excited band due to rapid thermalization. They transfer narrowband excitation to the reaction center (13). We adopt the level schemes of Fig. 2 *B* and *E* to describe collective excitations in molecular aggregates and show that quantum coherence may increase the efficiency of photosynthesis. We demonstrate that the photosynthetic reaction center may be viewed as a biological quantum heat engine (BQHE) that transforms high-energy thermal photon radiation into low-entropy electron flux (Fig. 2*A*, adapted from ref. 31) and estimate the role of noise-induced quantum

Author contributions: K.E.D., D.V.V., S.M., and M.O.S. designed research; K.E.D. and D.V.V. performed research; and K.E.D., D.V.V., S.M., and M.O.S. wrote the paper.

The authors declare no conflict of interest.

This article is a PNAS Direct Submission.

See Commentary on page 2693.

[1]To whom correspondence may be addressed. E-mail: dmitri.voronine@gmail.com or kdorfman@uci.edu.

This article contains supporting information online at www.pnas.org/lookup/suppl/doi:10.1073/pnas.1212666110/-/DCSupplemental.

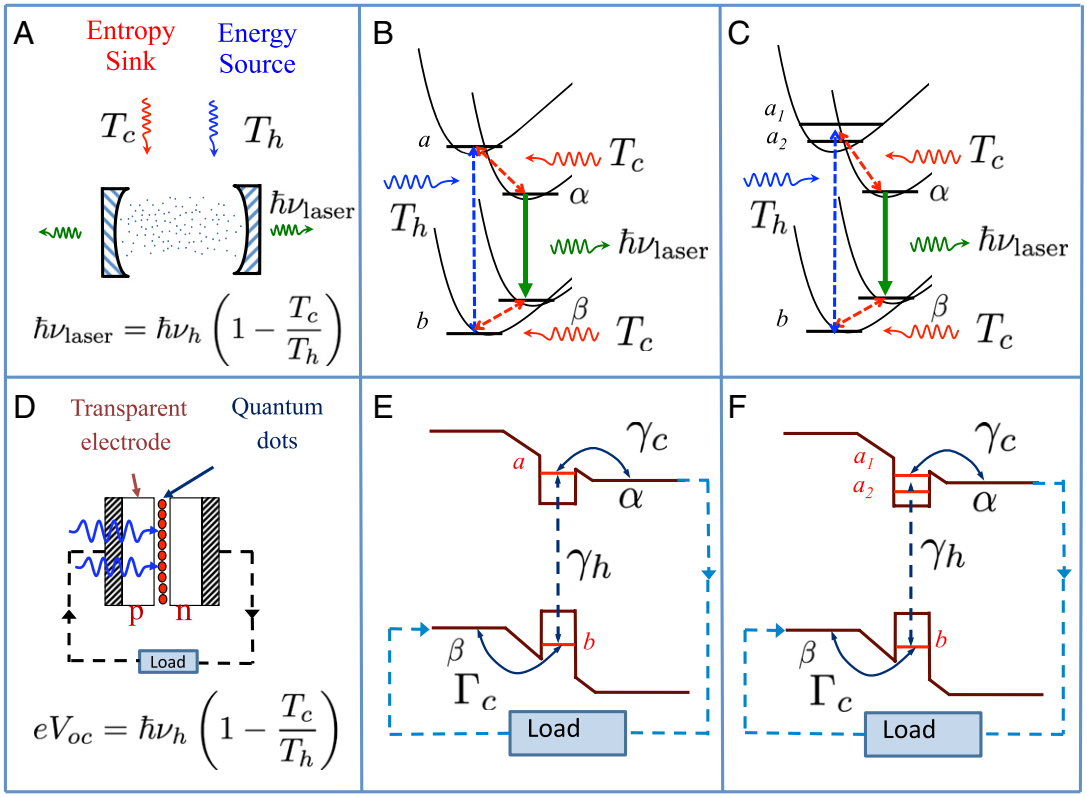

Fig. 1. Schemes of a laser QHE (*A*) and a photocell QHE consisting of quantum dots sandwiched between *p*- and *n*-doped semiconductors (*D*). These QHEs are pumped by hot photons at temperature T_h (energy source, blue) and by cold photons or phonons at temperature T_c (entropy sink, red) and operate with quantum efficiency governed by the Carnot relation. Schemes of four-level molecules inside the laser cavity (*B*) and electronic states of the quantum dot photocell (*E*). Optical transitions $b \leftrightarrow a$ and $a \leftrightarrow \alpha$ ($b \leftrightarrow \beta$) are driven by "hot" photons and ambient "cold" phonons, respectively. *C* and *F* are the same as *B* and *E*, respectively, with the upper level *a* replaced by two levels a_1 and a_2. The QHE power of the five-level system in *C* and *F* can be doubled compared with the four-level system in *B* and *E* when there is coherence between these levels.

coherence on the efficiency of charge separation. This insight leads to a unified picture of two seemingly unrelated quantum coherence effects: oscillation of populations and enhanced electric current in the BQHE. The ultimate efficiency is bound by the Carnot limit, consistent with the second law of thermodynamics.

We describe the photoinduced charge separation between the donor *D* and the acceptor *A* molecules interacting with thermal light (Fig. 2*B*) using the four-level QHE scheme shown in Fig. 2*E*. State *b* corresponds to the lowest energy configuration where both molecules are in the ground states. State *a* describes the configuration where donor *D* is excited (both the excited electron and the hole are in donor *D*); α is a charge-separated state with the electron in acceptor *A* and the hole in donor *D*. Finally, β is the ionized state where the electron is transferred to a "sink" and the system is positively charged. After absorption of a solar photon, the excited electron is promoted from *b* to *a* and is then transferred to α with the excess energy radiated as a phonon. Furthermore, the electron released from state α results in a current from α to β, which we model by a relaxation rate Γ, such that the current $j = e\Gamma\rho_{\alpha\alpha}$ is governed by the population of α. To complete the cycle, we assume that another population transfer takes place which brings the electron back to the ground state *b* of donor *D* with emission of a phonon with excess energy.

Quantum coherence can significantly affect the efficiency of this process. Fig. 2*C* shows two closely spaced identical donor molecules D_1 and D_2 that represent a special pair of chlorophylls at the heart of the reaction center complex where the primary charge separation takes place (22). In photosynthesis, the sunlight absorbed by antennae complexes is consequently transferred to the special pair. In our setup, we exclude the antenna and assume that the pair absorbs sunlight cooperatively via the exciton states a_1 and a_2 which are separated by the Davydov splitting (33). In bacterial systems the splitting is on the order of 450–800 wavenumbers (43), whereas in the Photosystem II reaction center, the special pair coupling is weaker (160–200 cm^{-1}) (21). The remaining states are similar to those of Fig. 2*E*. As was shown in refs. 9 and 10, the model in Fig. 2*F* can exhibit noise-induced quantum coherence due to Fano interference. This effect originates from the coupling of two levels to the same continuum (4). The initial excitation of states a_1 and a_2 can be transferred to the acceptor molecule in state α by emission of a phonon and can produce useful work by contributing to the electric current and returning to *b* via β. On the other hand, the system can return to *b* via stimulated or spontaneous emission. Fano interference can minimize the latter process by inducing coherence between a_1 and a_2 (*SI Text*). Then the net absorption is enhanced and the electron flux is increased.

Identifying the primary electron donors and dominating charge-separation pathways has been a question of recent extensive research and debate. At the moment, there is much evidence that two main pathways make significant contributions under ambient conditions and the lowest energy states depend on disorder (44–47). Whereas in bacterial reaction centers the primary charge separation takes place at the special pair (as used in this work), the reaction centers of Photosystem II also use an additional pathway which starts at the accessory chlorophyll of the *D*1 branch (48, 49). In this work we discuss only the first pathway, which is present in both types of reaction centers and plays an important role in optimizing the electron transfer efficiency. Using design principles inspired by

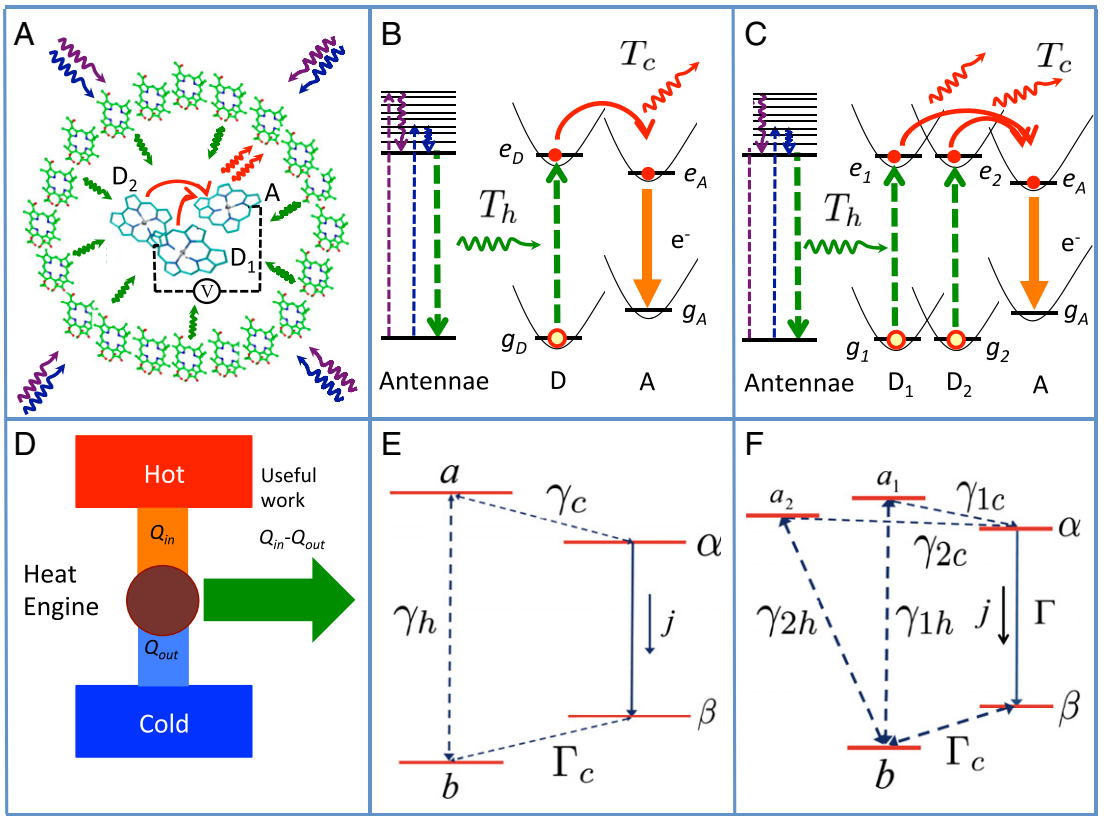

Fig. 2. Schemes of a BQHE based on the photosynthetic reaction center (*A*) and a generic heat engine (*D*). Scheme of charge separation between a donor *D* and an acceptor *A* molecule (*B*). The broad solar spectrum is absorbed by the antennae complexes (arranged in a circle in *A*) which undergo rapid thermalization due to phonon scattering and reach the bottom of the electronic band. Thus, the narrowband excitation is transferred to the reaction center represented by donor and acceptor molecules. *E* represents the generic four-level QHE scheme. *C* and *F* are the same as *B* and *E*, respectively, except that the upper level *a* is replaced by two levels a_1 and a_2 separated by Davydov splitting. The power delivered by the QHE of *C* and *F* can be doubled compared with *B* and *E* if there is coherence between levels a_1 and a_2.

nature, we propose a scheme to design artificial light-harvesting molecular complexes with increased electron transfer efficiency.

The effects of noise-induced coherence can be illustrated by the following equation for the population of state a_1 (50):

$$\dot{\rho}_{11} = -\gamma_{1c}\left[(1+\overline{n}_{1c})\rho_{11} - \overline{n}_{1c}\rho_{\alpha\alpha}\right] - \gamma_{1h}\left[(1+\overline{n}_{1h})\rho_{11} - \overline{n}_{1h}\rho_{bb}\right] - \left[\gamma_{12c}(\overline{n}_{2c}+1) + \gamma_{12h}(\overline{n}_{2h}+1)\right](\rho_{21}+\rho_{12}), \quad [1]$$

where the ρ_{ii} are the populations of levels i, and $\overline{n}_h(\overline{n}_c)$ are the average number of hot solar photons (cold ambient phonons); $\gamma_{1c}(\gamma_{1h})$ are the decay rates from the upper level to levels α and b, respectively; and $\gamma_{12h}(\gamma_{12c})$ are cross-couplings that describe the effect of interference.* The complete set of equations of motion which describe the evolution of all density matrix elements is given in *SI Text*. To obtain a clear physical insight and a qualitative estimate, we consider a simplified model and neglect memory effects (Markov approximation) under the condition of weak system–bath coupling. Future extension to the non-Markovian regime will be necessary to provide a more precise, quantitative calculation of the predicted effects. Recent work has suggested that protein environment plays an important role in photosynthesis (51). The complicated dynamics of strongly coupled protein bath goes beyond the scope of our paper.

*Maximum coherence $\gamma_{12c} = \sqrt{\gamma_{1c}\,\gamma_{2c}}$ and $\gamma_{12h} = \sqrt{\gamma_{1h}\,\gamma_{2h}}$; no coherence $\gamma_{12c} = \gamma_{12h} = 0$.

We construct the model in Fig. 2*F* using elements of the reaction center (*SI Text*). Charge separation in a reaction center can be considered as work done by a system similarly to a photovoltaic cell or more generally a QHE powered by thermal radiation of the sun (10). Assuming that α and β are connected by a "load," we introduce the concept of effective voltage V as a drop of the electrostatic potential across the load, which, according to Fermi–Dirac statistics, yields $eV = E_\alpha - E_\beta + k_B T_\alpha \log(\rho_{\alpha\alpha}/\rho_{\beta\beta})$, where E_i is the energy of the state i and e is the electric charge. We apply

Table 1. Summary of the three parameter regimes

	I (Overdamped)	II (Underdamped)	III (Intermediate)
$E_1 - E_2$, cm^{-1}	120	600	720
$E_1 - E_b$, cm^{-1}	14,856	14,856	14,856
$E_1 - E_c$, cm^{-1}	1,611	1,611	1,611
$E_v - E_b$, cm^{-1}	1,611	1,611	1,611
T_s, K	6,000	6,000	6,000
T_a, K	300	300	300
γ_{1h}, cm^{-1}	0.005	0.005	0.005
γ_{2h}, cm^{-1}	0.0016	0.005	0.005
γ_{1c}, cm^{-1}	140	35	280
γ_{2c}, cm^{-1}	18	35	280
Γ_c, cm^{-1}	200	50	300
$1/\tau_2$, cm^{-1}	41	41	41
n_{1h}	60,000	10,000	90,000
n_{2h}	10,000	20,000	10,000

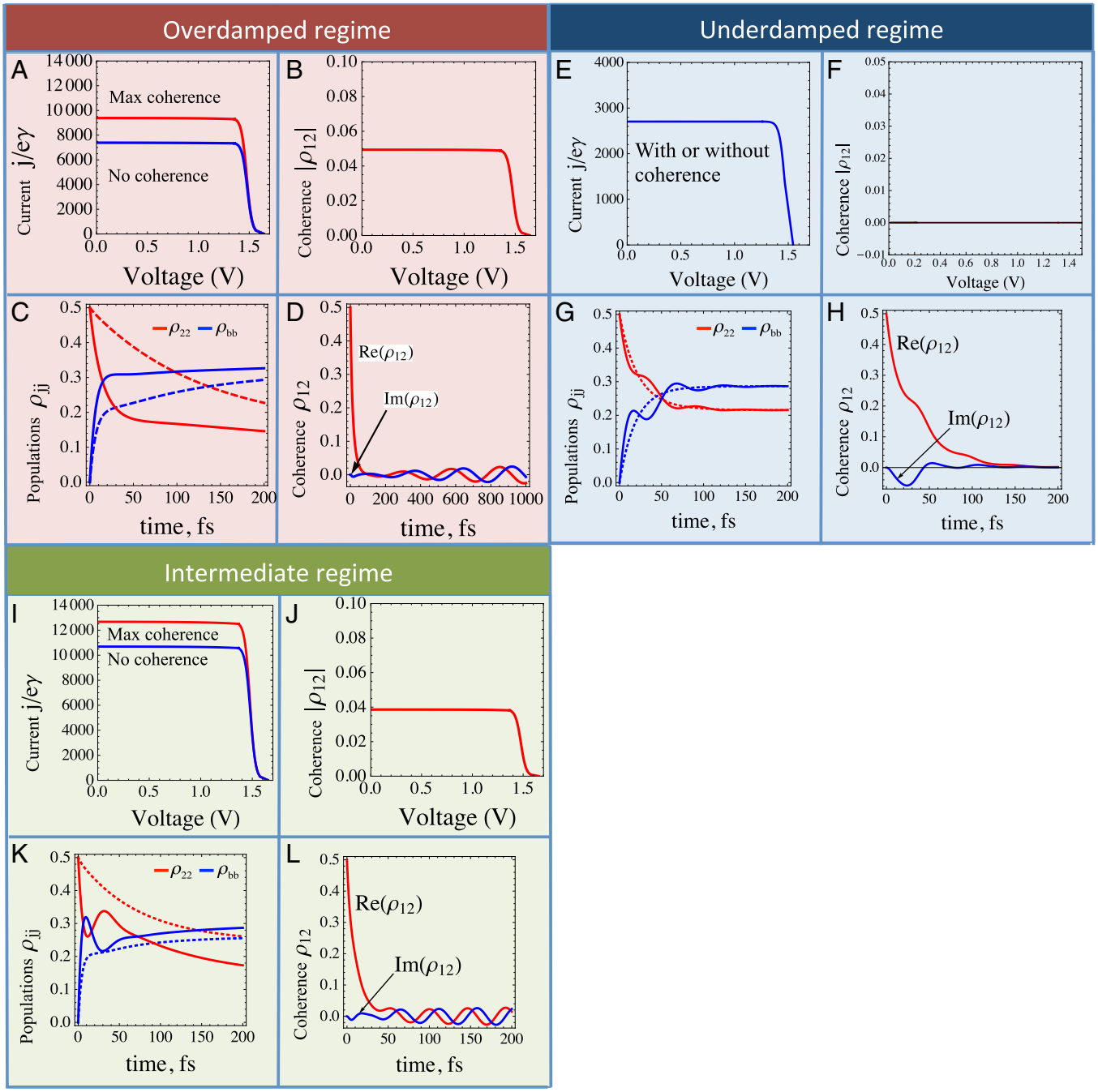

Fig. 3. Steady-state characteristics and excited-state dynamics of a BQHE model of a photosynthetic reaction center in Fig. 2*F*. Three regimes are shown: overdamped (*A–D*); underdamped (*E–H*), and intermediate (*I–L*). Quantum coherence can enhance the electric current by up to 27% in the overdamped and 18% in the intermediate regimes compared with the same five-level system without coherence, whereas no current enhancement is achieved in the underdamped regime. Nonzero steady-state coherence is obtained in *B* and *J*. Populations reveal oscillations in the presence of coherence in *G* and *K* (solid lines), whereas no oscillations are present without coherence (dashed lines). Long-lived coherence is obtained in the overdamped (*D*) and intermediate (*L*) regimes. Parameters corresponding to different regimes are summarized in Table 1 (*Methods*).

this to the steady-state regime and calculate the populations $\rho_{\alpha\alpha}$ and $\rho_{\beta\beta}$ at sufficiently long times. For the operation near the open circuit (weak illumination, no current) the power acquired from the sun is $P_S = j \cdot (E_a - E_b)/e$, whereas the power that can be extracted from the reaction center is $P = j \cdot V_{oc}$. Therefore, the efficiency of such a heat engine $\eta = P/P_S = 1 - T_a/T_S$ is given by the Carnot relation.

Noise-induced coherence is most pronounced if the two interfering levels overlap, i.e., the level spacing is small compared with the inverse lifetimes of a_1 and a_2. In this case, the populations relax exponentially to the steady state. In the opposite limit, quantum coherence manifests itself as oscillations of populations of eigenstates (8, 31). These two limits can be understood by using a simple analogy with the overdamped and underdamped regimes of a harmonic oscillator. Thus, one can associate the enhancement of the steady-state yield with the overdamped regime and population oscillations with the underdamped regime. It is remarkable that both effects are caused by the same mechanism of noise-

induced coherence but realized for different parameters. The summary of parameters used in our simulations is listed in Table 1 of *Methods*. We focus on the Photosystem II reaction center and perform specific simulations using well-known parameters from recent literature (20, 21, 31). We also simulate artificial systems with a broad range of parameters to demonstrate related coherence effects.

We next calculate steady-state current–voltage characteristics for our BQHE model (Fig. 2*F*) in the overdamped regime by increasing the rate Γ from zero (open circuit) to the short-circuit condition (no electrostatic potential across the load). Fig. 3 *A* and *B* depict the normalized electric current and the steady-state coherence ρ_{12} (absolute value), respectively, as a function of the voltage. The red line corresponds to the maximum coherence, whereas the blue line is obtained with no coherence. In this example, noise-induced coherence increases the peak power by about 27% compared with the same five-level system without coherence. The dynamics of populations and coherence ρ_{12} shown in Fig. 3 *C* and *D*, respectively, demonstrate that in this regime there are no population oscillations, whereas coherence oscillates and reaches a steady state.

Fig. 3 *G* and *H* show the population and coherence dynamics, respectively, in the underdamped regime. The oscillatory behavior of populations and coherence is clearly observed on a time scale of $\sim$ 130 fs. This corresponds to the decoherence time after which populations reach the steady-state values as expected for a closed system with a conserved probability. In the absence of coherence, populations evolve exponentially and reach the steady state at nearly the same time as in the presence of coherence. In the underdamped oscillator regime, there is no steady-state coherence (Fig. 3 *E* and *F*) and thus there is no enhancement of the steady-state electric current.

Finally, we investigate the intermediate damping regime where both population oscillations and an enhanced current yield can coexist. Fig. 3 *I* and *J* show the steady-state current–voltage characteristics and coherence as a function of the voltage drop across the acceptor load, respectively. Even for moderate coherence ($\rho_{12} \sim 0.04$), there is an enhancement of 18% in the yield. On the other hand the dynamics of populations and coherence shown in Fig. 3 *K* and *L*, respectively, reveals large-amplitude oscillations on a time scale of $\sim$ 130 fs. Small-amplitude long-lived (steady-state) oscillations of coherences are also present in this regime.

In summary, we describe QHEs inspired by photosynthesis that operate under the natural conditions of incoherent excitation by sunlight using the formalism developed earlier for the laser and photocell engines. This establishes a connection between two previously unrelated effects attributed to quantum coherence: population oscillations in photosynthetic complexes and enhanced photocurrent yield in QHEs. We investigate parameter regimes where large electric current yield enhancement and/or population oscillations are observed and identify noise-induced quantum coherence as the common origin of these effects. In contrast with studies where coherence was generated by laser radiation, this noise-induced coherence requires no external source. Our simulations show that the coherence builds up on a time scale of a few femtoseconds and reaches a steady state in a few nanoseconds. Zero current (open circuit) results in zero coherence whereas steady-state coherence can lead to current enhancement. We find that the structure of the special pair in photosynthetic reaction centers is suitable to use these quantum effects and increase the efficiency of charge separation. Similar noise-induced coherence effects have been experimentally demonstrated in semiconductor quantum wells (52, 53). Our study suggests that these experiments may be extended to photosynthetic complexes and hold promise for improving the design and boosting the efficiencies of light-harvesting devices. A broad range of parameter regimes provides flexibility in designs and materials.

Methods

We use a quantum master equation approach similar to earlier photocell work (*SI Text*) to derive the evolution of the density matrix and obtain steady-state characteristics such as the quantum yield and the electric current. For the simulations shown in Fig. 3 we use the parameters listed in Table 1. Here, $E_1 - E_b$ and $E_1 - E_c$ ($E_v - E_b$) are the transition energies for photons and phonons, respectively; $1/\tau_2$ is the decoherence rate. We assume that the system is irradiated by a concentrated solar radiation with an average number of photons n_{1h} and n_{2h} at energies $E_1 - E_b$ and $E_2 - E_b$, respectively. Due to the large phonon energy (1,611 cm^{-1}) that results in small occupation numbers, we neglect stimulated processes associated with phonons at room temperature. n_{1c} and n_{2c} were set to zero.

ACKNOWLEDGMENTS. K.E.D., D.V.V., and M.O.S. acknowledge the support by National Science Foundation (NSF) Grants PHY-1241032 (INSPIRE CREATIV) and EEC-0540832 (MIRTHE ERC), the Office of Naval Research, and Robert A. Welch Foundation Award A-1261. S.M. acknowledges support from NSF Grant CHE-1058791, Defense Advanced Research Planning Agency BAA-10-40 QuBE, and the Chemical Sciences, Geosciences and Biosciences Division, Office of Basic Energy Sciences, Office of Science, US Department of Energy.

1. Scovil HED, Schulz-DuBois EO (1959) Three-level masers as heat engines. *Phys Rev Lett* 2(6):262–263.
2. Scully MO, Zubairy MS, Agarwal GS, Walther H (2003) Extracting work from a single heat bath via vanishing quantum coherence. *Science* 299(5608):862–864.
3. Einstein A (1917) Zur Quantentheorie der Strahlung. *Phys Z* 18:121–128.
4. Harris SE (1989) Lasers without inversion: Interference of lifetime-broadened resonances. *Phys Rev Lett* 62(9):1033–1036.
5. Scully MO, Zubairy MS (1997) *Quantum Optics* (Cambridge Univ Press, Cambridge, England).
6. Kozlov VV, Rostovtsev Y, Scully MO (2006) Inducing quantum coherence via decays and incoherent pumping with application to population trapping, lasing without inversion, and quenching of spontaneous emission. *Phys Rev A* 74(6):063829.
7. Scully MO (2010) Quantum photocell: Using quantum coherence to reduce radiative recombination and increase efficiency. *Phys Rev Lett* 104(20):207701.
8. Dorfman KE, Jha PK, Das S (2011) Quantum-interference-controlled resonance profiles from lasing without inversion to photodetection. *Phys Rev A* 84(5):053803.
9. Scully MO, Chapin KR, Dorfman KE, Kim MB, Svidzinsky AA (2011) Quantum heat engine power can be increased by noise-induced coherence. *Proc Natl Acad Sci USA* 108(37):15097–15100.
10. Svidzinsky AA, Dorfman KE, Scully MO (2011) Enhancing photovoltaic power by Fano-induced coherence. *Phys Rev A* 84(5):053818.
11. Shockley W, Queisser HJ (1961) Detailed balance limit of efficiency of p-n junction solar cells. *J Appl Phys* 32(3):510–519.
12. Fingerhut BP, Zinth W, de Vivie-Riedle R (2010) The detailed balance limit of photochemical energy conversion. *Phys Chem Chem Phys* 12(2):422–432.
13. Blankenship RE, et al. (2011) Comparing photosynthetic and photovoltaic efficiencies and recognizing the potential for improvement. *Science* 332(6031):805–809.
14. Caruso F, Chin AW, Datta A, Huelga SF, Plenio MB (2009) Highly efficient energy excitation transfer in light-harvesting complexes: The fundamental role of noise-assisted transport. *J Chem Phys* 131(10):105106.
15. Rebentrost P, Mohseni M, Kassal I, Lloyd S, Aspuru-Guzik A (2009) Environment-assisted quantum transport. *New J Phys* 11:033003.
16. Scholes GD (2010) Quantum-coherent electronic energy transfer: Did nature think of it first? *J. Phys. Chem. Lett.* 1(1):2–8.
17. Ishizaki A, Fleming GR (2009) Theoretical examination of quantum coherence in a photosynthetic system at physiological temperature. *Proc Natl Acad Sci USA* 106(41): 17255–17260.
18. Lloyd S, Mohseni M (2010) Symmetry-enhanced supertransfer of delocalized quantum states. *New J Phys* 12:075020.
19. Strümpfer J, Sener M, Schulten K (2012) How quantum coherence assists photosynthetic light-harvesting. *J Phys Chem Lett* 3(4):536–542.
20. Abramavicius D, Mukamel S (2010) Energy-transfer and charge-separation pathways in the reaction center of photosystem II revealed by coherent two-dimensional optical spectroscopy. *J Chem Phys* 133(18):184501.
21. Madjet ME, Abdurahman A, Renger T (2006) Intermolecular coulomb couplings from ab initio electrostatic potentials: Application to optical transitions of strongly coupled pigments in photosynthetic antennae and reaction centers. *J Phys Chem B* 110(34): 17268–17281.
22. Deisenhofer J, Epp O, Miki K, Huber R, Michel H (1985) Structure of the protein subunits in the photosynthetic reaction centre of Rhodopseudomonas viridis at 3Å resolution. *Nature* 318(6047):618–624.
23. Engel GS, et al. (2007) Evidence for wavelike energy transfer through quantum coherence in photosynthetic systems. *Nature* 446(7137):782–786.
24. Collini E, et al. (2010) Coherently wired light-harvesting in photosynthetic marine algae at ambient temperature. *Nature* 463(7281):644–647.

25. Panitchayangkoon G, et al. (2010) Long-lived quantum coherence in photosynthetic complexes at physiological temperature. *Proc Natl Acad Sci USA* 107(29): 12766–12770.
26. Brixner T, et al. (2005) Two-dimensional spectroscopy of electronic couplings in photosynthesis. *Nature* 434(7033):625–628.
27. Abramavicius D, Palmieri B, Voronine DV, Sanda F, Mukamel S (2009) Coherent multidimensional optical spectroscopy of excitons in molecular aggregates; quasiparticle versus supermolecule perspectives. *Chem Rev* 109(6):2350–2408.
28. Harel E, Engel GS (2012) Quantum coherence spectroscopy reveals complex dynamics in bacterial light-harvesting complex 2 (LH2). *Proc Natl Acad Sci USA* 109(3):706–711.
29. Schlau-Cohen GS, et al. (2012) Elucidation of the timescales and origins of quantum electronic coherence in LHCII. *Nat Chem* 4(5):389–395.
30. Scholes GD, Fleming GR, Olaya-Castro A, van Grondelle R (2011) Lessons from nature about solar light harvesting. *Nat Chem* 3(10):763–774.
31. Abramavicius D, Mukamel S (2010) Quantum oscillatory exciton migration in photosynthetic reaction centers. *J Chem Phys* 133(6):064510.
32. Panitchayangkoon G, et al. (2011) Direct evidence of quantum transport in photosynthetic light-harvesting complexes. *Proc Natl Acad Sci USA* 108(52):20908–20912.
33. Davydov AS (1962) *Theory of Molecular Excitons* (McGraw-Hill, New York).
34. Kenkre VM, Reineker P (1982) *Exciton Dynamics in Molecular Crystals and Aggregates* (Springer, Berlin).
35. Haken H, Strobl G (1967) Exact treatment of coherent and incoherent triplet exciton migration. *The Triplet State*, ed Zahlan AB (Cambridge Univ Press, Cambridge), p 311.
36. Mukamel S (2010) Communications: Signatures of quasiparticle entanglement in multidimensional nonlinear optical spectroscopy of aggregates. *J Chem Phys* 132(24): 241105.
37. Nalbach P, Braun D, Thorwart M (2011) Exciton transfer dynamics and quantumness of energy transfer in the Fenna-Matthews-Olson complex. *Phys Rev E Stat Nonlin Soft Matter Phys* 84(4 Pt 1):041926.
38. Christensson N, Kauffmann HF, Pullerits T, Mančal T (2012) Origin of long-lived coherences in light-harvesting complexes. *J Phys Chem B* 116(25):7449–7454.
39. Chin AW, Huelga SF, Plenio MB (2012) Coherence and decoherence in biological systems: Principles of noise-assisted transport and the origin of long-lived coherences. *Philos Trans Math Phys Eng Sci* 370(1972):3638–3657.
40. Turner DB, Wilk KE, Curmi PMG, Scholes GD (2011) Comparison of electronic and vibrational coherence measured by two-dimensional electronic spectroscopy. *J. Phys. Chem. Lett.* 2(15):1904–1911.
41. Zhang WM, Meier T, Chernyak V, Mukamel S (1998) Exciton-migration and three-pulse femtosecond optical spectroscopies of photosynthetic antenna complexes. *J Chem Phys* 108:7763.
42. Mukamel S (1995) *Principles of Nonlinear Optical Spectroscopy* (Oxford Univ Press, New York).
43. Won Y, Friesner RA (1988) Theoretical study of photochemical hole burning in photosynthetic bacterial reaction centers. *J Phys Chem* 92(8):2208–2214.
44. Novoderezhkin VI, Dekker JP, van Grondelle R (2007) Mixing of exciton and charge-transfer states in Photosystem II reaction centers: Modeling of Stark spectra with modified Redfield theory. *Biophys J* 93(4):1293–1311.
45. Romero E, van Stokkum IHM, Novoderezhkin VI, Dekker JP, van Grondelle R (2010) Two different charge separation pathways in photosystem II. *Biochemistry* 49(20): 4300–4307.
46. Novoderezhkin VI, Romero E, Dekker JP, van Grondelle R (2011) Multiple charge-separation pathways in photosystem II: Modeling of transient absorption kinetics. *ChemPhysChem* 12(3):681–688.
47. Cardona T, Sedoud A, Cox N, Rutherford AW (2012) Charge separation in photosystem II: A comparative and evolutionary overview. *Biochim Biophys Acta* 1817(1): 26–43.
48. Holzwarth AR, et al. (2006) Kinetics and mechanism of electron transfer in intact photosystem II and in the isolated reaction center: Pheophytin is the primary electron acceptor. *Proc Natl Acad Sci USA* 103(18):6895–6900.
49. Renger T, Schlodder E (2010) Primary photophysical processes in photosystem II: Bridging the gap between crystal structure and optical spectra. *ChemPhysChem* 11(6):1141–1153.
50. Power EA (1964) *Introductory Quantum Electrodynamics* (Elsevier, New York).
51. Lee H, Cheng YC, Fleming GR (2007) Coherence dynamics in photosynthesis: Protein protection of excitonic coherence. *Science* 316(5830):1462–1465.
52. Faist J, Capasso F, Sirtori C, West KW, Pfeiffer LN (1997) Controlling the sign of quantum interference by tunneling from quantum wells. *Nature* 390:589.
53. dell'Orto T, Almeida J, Coluzza C, Margaritondo G, Margaritondo G; Di Ventra M (1995) Evidence for a photocurrent Fano resonance in an artificial nanostructure. *Phys Rev B Condens Matter* 52(4):R2265–R2268.